Computers and Concrete, *Vol.15, No.3 (2015) 373-389*
DOI: http://dx.doi.org/10.12989/cac.2015.15.3.373

Numerical modelling of nonlinear behaviour of prestressed concrete continuous beams

Tiejiong Lou[1], Sergio M.R. Lopes[*1] and Adelino V. Lopes[2]

[1]*CEMUC, Department of Civil Engineering, University of Coimbra, Coimbra 3030-788, Portugal*
[2]*Department of Civil Engineering, University of Coimbra, Coimbra 3030-788, Portugal*

(*Received July 3, 2013, Revised January 11, 2015, Accepted January 18, 2015*)

Abstract. The development of a finite element model for the geometric and material nonlinear analysis of bonded prestressed concrete continuous beams is presented. The nonlinear geometric effect is introduced by the coupling of axial and flexural fields. A layered approach is applied so as to consider different material properties across the depth of a cross section. The proposed method of analysis is formulated based on the Euler-Bernoulli beam theory. According to the total Lagrangian description, the constructed stiffness matrix consists of three components, namely, the material stiffness matrix reflecting the nonlinear material effect, the geometric stiffness matrix reflecting the nonlinear geometric effect and the large displacement stiffness matrix reflecting the large displacement effect. The analysis is capable of predicting the nonlinear behaviour of bonded prestressed concrete continuous beams over the entire loading stage up to failure. Some numerical examples are presented to demonstrate the validity and applicability of the proposed model.

Keywords: prestressed concrete beams; finite element; material nonlinearity; geometric nonlinearity; behaviour

1. Introduction

The application of pre- and post-tensioning techniques to continuous concrete members is very common in engineering practices. Because of continuity, the behaviour of continuous prestressed concrete members can be quite different from that of simply-supported ones. Although extensive works have been carried out to study the behaviour of prestressed concrete continuous members (Kulprapha and Warnitchai 2012; Lee *et al*. 2004; Lou *et al*. 2013a, 2014a,b; Naito *et al*. 2008; Rana *et al*. 2013; Turmo *et al*. 2011), there is still a lack of understanding of some aspects of behaviour of these members. For example, the prestress secondary moments in the inelastic range have been a subject of much controversy, and no agreement has yet been reached. In addition, the behaviour of moment redistribution in continuous prestressed concrete members is another interesting subject that needs to be further investigated, especially when the members are made of high-strength concrete and/or prestressed with fibre reinforced polymer tendons for the brittleness of these materials (Ho and Zhou 2011; Roth *et al*. 2010; Schmidt *et al*. 2012).

Because the experimental work on the continuous prestressed concrete members is rather

∗Corresponding author, Professor, E-mail: sergio@dec.uc.pt

 ISSN: 1598-8198 (Print), 1598-818X (Online)

expensive, it is practically difficult to fabricate and test a large number of continuous specimens in one experimental programme. Therefore, the development of a reliable and powerful computer model, which is capable of simulating the comprehensive behaviour of prestressed concrete continuous members, is necessary. The finite element method affords an effective numerical technique to approximate closely the real behaviour of a member. In the finite element idealization of reinforced and prestressed concrete beams, the one-dimensional model, in which the member is idealized as an assemblage of beam elements interconnected at nodes, has been usually preferred by researchers for its simplicity and computer efficiency (Al-Sadder *et al*. 2006; Campbell and Kodur 1990; Lou *et al*. 2013b; Markovic *et al*. 2013). Campbell and Kodur (1990) developed a macroscopic model based on the moment-curvature relationship pregenerated through section analysis. The model can take care of continuous bonded prestressed concrete rectangular, T or I beams subjected to concentrated or uniform loading, and has been applied to the evaluation of moment redistribution in these beams (Kodur and Campbell 1996, 1999). However, this model did not take into account the geometric nonlinearity that may have important influence on the slender beams that are generally true for prestressed continuous beams.

This paper presents a finite element model developed to predict the nonlinear behaviour of bonded prestressed concrete continuous beams throughout all ranges of loading up to failure. Both the geometric and material nonlinearities are considered. The Euler-Bernoulli beam theory is utilized to establish the finite element formulation. This theory, as opposed to the Timoshenko beam theory (Lou *et al*. 2014c), is well applicable to slender beams where the shear deformations are negligible. The proposed model is verified with the experimental results of continuous beam specimens available in literature. Some typical aspects of inelastic behaviour of the continuous beams are examined.

2. Material models

The stress-strain ($\sigma_c - \varepsilon_c$) relationship for concrete in compression is simulated using the EC2 equation (CEN 2004):

$$\frac{\sigma_c}{f_{cm}} = \frac{k\eta - \eta^2}{1 + (k-2)\eta} \tag{1}$$

where f_{cm} is the mean compressive strength (in MPa), and $f_{cm} = f_{ck} + 8$; f_{ck} is the characteristic cylinder compressive strength (in MPa); $\eta = \varepsilon_c / \varepsilon_{c0}$; $k = 1.05 E_c \varepsilon_{c0} / f_{cm}$; ε_{c0} is the concrete strain at peak stress and $\varepsilon_{c0}(‰) = 0.7 f_{cm}^{0.31}$; E_c is the concrete modulus of elasticity (in GPa), and $E_c = 22(f_{cm}/10)^{0.3}$. Eq. (1) is subject to the condition that the concrete strain is not higher than the ultimate compressive strain ε_u determined by

$$\varepsilon_u(‰) = 3.5 \quad \text{for} \quad f_{ck} < 50 \text{ MPa} \tag{2a}$$

$$\varepsilon_u(‰) = 2.8 + 27[(98 - f_{cm})/100]^4 \quad \text{for} \quad f_{ck} \geq 50 \text{ MPa} \tag{2b}$$

The concrete in tension is assumed to be linear elastic prior to cracking, followed by linear tension stiffening behaviour. The stress-strain relationship is expressed as follows:

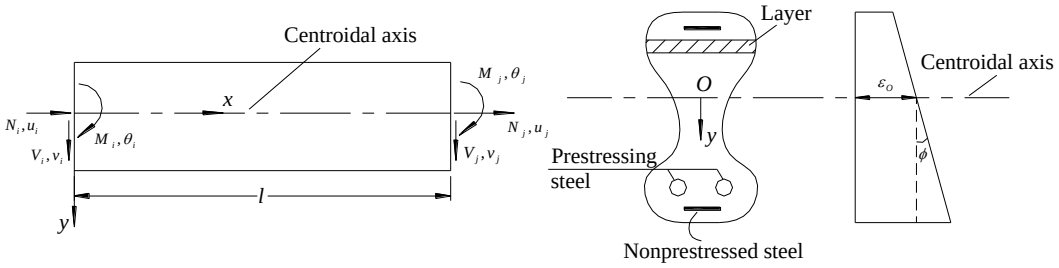

Fig. 1 Element, section and strain: (a) beam element; (b) layered section; (c) section strain

$$\text{Prior to cracking,}\quad \sigma_c = E_c \varepsilon_c \tag{3a}$$

$$\text{After cracking,}\quad \sigma_c = f_t \left[1 - \frac{\varepsilon_c - \varepsilon_{cr}}{\varepsilon_{tu} - \varepsilon_{cr}} \right] \tag{3b}$$

where f_t is the concrete tensile strength; $\varepsilon_{cr} = f_t / E_c$; and ε_{tu} is the concrete tensile strain corresponding to zero stress, which is used to include the effects of tension stiffening. According to EC2, the tensile strength f_t is calculated from

$$f_t = 0.3 f_{ck}^{2/3} \quad \text{for concrete class not higher than C50/60} \tag{4a}$$

$$f_t = 2.12 \ln(1 + f_{cm}/10) \quad \text{for concrete class higher than C50/60} \tag{4b}$$

The stress-strain ($\sigma_p - \varepsilon_p$) curve for prestressing steel proposed by Menegotto and Pinto (1973) is used in this study. It is expressed as follows:

$$\sigma_p = E_p \varepsilon_p \left[Q + \frac{1 - Q}{\{1 + [\varepsilon_p E_p / (K f_{py})]^R\}^{1/R}} \right] \le f_{pu} \tag{5}$$

where E_p, f_{py} and f_{pu} are the modulus of elasticity, yield stress and ultimate strength of prestressing steel, respectively; and K, Q and R are the empirical parameters depending on the type of prestressing steel. For Grade 270 strands, the values of K, Q and R are 1.0618, 0.01174 and 7.344, respectively; and for Grade 235 wires, the values are 1.0325, 0.00625 and 6.06, respectively.

The nonprestressed steel is assumed to be elastic-perfectly plastic in both tension and compression, and the stress-strain ($\sigma_s - \varepsilon_s$) relationship is expressed as follows:

$$\text{At elastic range,}\quad \sigma_s = E_s \varepsilon_s \tag{6a}$$

$$\text{After yielding,}\quad \sigma_s = f_y \tag{6b}$$

where E_s is the nonprestressed steel modulus of elasticity; and f_y is the nonprestressed steel yield strength.

3. Finite element formulation

Consider a two-nodal plane beam element with properties to be described in the local coordinate system (*x*,*y*), as shown in Fig. 1(a). Each node has three degrees of freedom: axial displacement *u*, transverse displacement *v*, and rotation θ. Assuming that the axial and transverse displacements are a linear function and a cubic polynomial, respectively, and that the shear deformations are negligible, the axial strain ε_O and section curvature ϕ are related to the element nodal displacements $\boldsymbol{u}^e$ by

$$\begin{Bmatrix} \varepsilon_O \\ \phi \end{Bmatrix} = (\boldsymbol{B}_L + \boldsymbol{B}_N / 2)\boldsymbol{u}^e \tag{7}$$

$$\boldsymbol{u}^e = \{u_i \quad v_i \quad \theta_i \quad u_j \quad v_j \quad \theta_j\}^T \tag{8}$$

$$\boldsymbol{B}_L = \begin{bmatrix} -\frac{1}{l} & 0 & 0 & \frac{1}{l} & 0 & 0 \\ 0 & \frac{6}{l^2}-\frac{12\xi}{l^2} & \frac{4}{l}-\frac{6\xi}{l} & 0 & -\frac{6}{l^2}+\frac{12\xi}{l^2} & \frac{2}{l}-\frac{6\xi}{l} \end{bmatrix} \tag{9a}$$

$$\boldsymbol{B}_N = \begin{bmatrix} 0 & \beta b_1 & \beta b_2 & 0 & \beta b_3 & \beta b_4 \\ 0 & 0 & 0 & 0 & 0 & 0 \end{bmatrix} \tag{9b}$$

$$b_1 = -\frac{6\xi}{l} + \frac{6\xi^2}{l};\ \ b_2 = 1 - 4\xi + 3\xi^2;\ \ b_3 = \frac{6\xi}{l} - \frac{6\xi^2}{l};\ \ b_4 = -2\xi + 3\xi^2 \tag{10}$$

$$\beta = b_1 v_i + b_2 \theta_i + b_3 v_j + b_4 \theta_j \tag{11}$$

where $\xi = x / l$; *l* is the length of the beam element.

The prestressing steel segment in each beam element is idealized to run parallel to the centroidal axis, with eccentricity equal to the average value of the eccentricities at two end nodes *i* and *j*, as shown in Fig. 2. This simplification ensures the identical cross section for an element, which is divided into a number of layers, as shown in Fig. 1(b). The layer number is dependent on the section shape and analysis precision required. In general, 10, 12 and 16 layers can be respectively used in a typical analysis for rectangular, T and I sections. The concrete strain in each layer is assumed to be uniformly distributed and equal to the strain at the centre of the layer. Assuming that a plane section remains plane after deformations and that perfect bond exists between the bonded steel and the surrounding concrete, that is, a linear distribution of strain on a cross section as shown in Fig. 1(c), the strain ε at any fibre of the section is given by

$$\varepsilon_c = \varepsilon_O + \phi y_c;\ \ \varepsilon_s = \varepsilon_O + \phi y_s;\ \ \varepsilon_p = \varepsilon_O + \phi y_p + \varepsilon_{p0} \tag{12}$$

where the subscripts *c*, *s*, *p* represent concrete, nonprestressed steel, and prestressing steel,

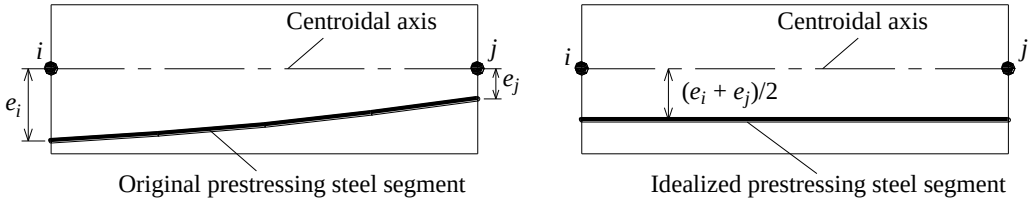

Fig. 2 Idealization of prestressing steel segment

respectively; ε_{p0} is the initial prestrain before prestress transfer. According to force equilibriums of the cross section, the axial force *N* and bending moment *M* can be expressed as follows:

$$\begin{Bmatrix} N \\ M \end{Bmatrix} = \begin{bmatrix} EA & EB \\ EB & EI \end{bmatrix} \begin{Bmatrix} \varepsilon_O \\ \phi \end{Bmatrix} + \begin{Bmatrix} N_0 \\ M_0 \end{Bmatrix} \tag{13}$$

$$EA = \sum_i E_{ci} A_{ci} + \sum_j E_{sj} A_{sj} + \sum_k E_{pk} A_{pk} \tag{14a}$$

$$EB = \sum_i E_{ci} A_{ci} y_{ci} + \sum_j E_{sj} A_{sj} y_{sj} + \sum_k E_{pk} A_{pk} y_{pk} \tag{14b}$$

$$EI = \sum_i E_{ci} A_{ci} y_{ci}^2 + \sum_j E_{sj} A_{sj} y_{sj}^2 + \sum_k E_{pk} A_{pk} y_{pk}^2 \tag{14c}$$

$$N_0 = \sum_k E_{pk} \varepsilon_{p0} A_{pk} \tag{15a}$$

$$M_0 = \sum_k E_{pk} \varepsilon_{p0} A_{pk} y_{pk} \tag{15b}$$

where the summation is made for all the layers of a material; *E* corresponds to the secant modulus of materials; *A* corresponds to the area; the subscripts *ci*, *sj* and *pk* correspond to the *i*th concrete layer, *j*th nonprestressed steel layer and *k*th prestressing steel layer, respectively.

By applying the principle of virtual works, the following equilibrium equations for an element can be established:

$$\boldsymbol{P}^e = \int_0^l (\boldsymbol{B}_L + \boldsymbol{B}_N)^T \begin{Bmatrix} N \\ M \end{Bmatrix} dx \tag{16}$$

$$\boldsymbol{P}^e = \{N_i \quad V_i \quad M_i \quad N_j \quad V_j \quad M_j\}^T \tag{17}$$

where $\boldsymbol{P}^e$ is the element equivalent nodal loads. Differentiating Eq. (16) with respect to $\boldsymbol{u}^e$ yields the element tangent stiffness equations:

$$d\boldsymbol{P}^e = \boldsymbol{K}_T^e d\boldsymbol{u}^e = (\boldsymbol{K}_1^e + \boldsymbol{K}_2^e + \boldsymbol{K}_3^e) d\boldsymbol{u}^e \tag{18}$$

where $\boldsymbol{K}_T^e$ is the element tangent stiffness matrix, which consist of three components, namely, the material stiffness matrix, $\boldsymbol{K}_1^e$, which represents the nonlinear material effect, the geometrical stiffness matrix, $\boldsymbol{K}_2^e$, which represents the nonlinear geometric effect, and the large displacement stiffness matrix, $\boldsymbol{K}_3^e$, which represents the large displacement effect. The explicit expressions for the submatrices are as follows (for *EA*, *EB* and *EI*, tangent moduli instead of scant moduli of materials are used):

$$\boldsymbol{K}_1^e = \begin{bmatrix} \frac{EA}{l} & 0 & -\frac{EB}{l} & -\frac{EA}{l} & 0 & \frac{EB}{l} \\ & \frac{12EI}{l^3} & \frac{6EI}{l^2} & 0 & \frac{-12EI}{l^3} & \frac{6EI}{l^2} \\ & & \frac{4EI}{l} & \frac{EB}{l} & -\frac{6EI}{l^2} & \frac{2EI}{l} \\ & & & \frac{EA}{l} & 0 & -\frac{EB}{l} \\ & \textit{Symmetry} & & & \frac{12EI}{l^3} & -\frac{6EI}{l^2} \\ & & & & & \frac{4EI}{l} \end{bmatrix} \tag{19a}$$

$$\boldsymbol{K}_2^e = N \begin{bmatrix} 0 & 0 & 0 & 0 & 0 & 0 \\ & \frac{6}{5l} & \frac{1}{10} & 0 & -\frac{6}{5l} & \frac{1}{10} \\ & & \frac{2l}{15} & 0 & -\frac{1}{10} & -\frac{l}{30} \\ & & & 0 & 0 & 0 \\ & \textit{Symmetry} & & & \frac{6}{5l} & -\frac{1}{10} \\ & & & & & \frac{2l}{15} \end{bmatrix} \tag{19b}$$

$$\boldsymbol{K}_3^e = \begin{bmatrix} 0 & a_1 & a_2 & 0 & -a_1 & a_3 \\ & a_4 & a_5 & -a_1 & -a_4 & a_6 \\ & & a_7 & -a_2 & -a_5 & a_8 \\ & & & 0 & a_1 & -a_3 \\ & \textit{Symmetry} & & & a_4 & -a_6 \\ & & & & & a_9 \end{bmatrix} \tag{19c}$$

$$a_1 = \frac{EA}{5}\left(\frac{-6v_i}{l^2} + \frac{6v_j}{l^2} - \frac{\theta_i}{2l} - \frac{\theta_j}{2l}\right) \tag{20a}$$

$$a_2 = \frac{EA}{5}\left(\frac{-v_i}{2l} + \frac{v_j}{2l} - \frac{2\theta_i}{3} + \frac{\theta_j}{6}\right) \tag{20b}$$

$$a_3 = \frac{EA}{5}\left(\frac{-v_i}{2l} + \frac{v_j}{2l} + \frac{\theta_i}{6} - \frac{2\theta_j}{3}\right) \tag{20c}$$

$$a_4 = \frac{6EB}{5l^2}(-\theta_i + \theta_j) + \frac{EA}{35}\left(\frac{72v_i^2}{l^3} - \frac{144v_iv_j}{l^3} + \frac{18v_i\theta_i}{l^2} + \frac{18v_i\theta_j}{l^2} + \frac{72v_j^2}{l^3}\right.$$
$$\left. - \frac{18v_j\theta_i}{l^2} - \frac{18v_j\theta_j}{l^2} + \frac{3\theta_i^2}{l} + \frac{3\theta_j^2}{l}\right) \tag{20d}$$

$$a_5 = \frac{EB}{5l}\left(\frac{3v_i}{l} - \frac{3v_j}{l} + \theta_i + 2\theta_j^2\right) + \frac{EA}{35}\left(\frac{9v_i^2}{l^2} - \frac{18v_iv_j}{l^2} + \frac{6v_i\theta_i}{l} + \frac{9v_j^2}{l^2}\right.$$
$$\left. - \frac{6v_j\theta_j}{l} - \frac{\theta_i^2}{4} + \frac{\theta_i\theta_j}{2} + \frac{\theta_j^2}{4}\right) \tag{20e}$$

$$a_6 = \frac{EB}{5l}\left(-\frac{3v_i}{l} + \frac{3v_j}{l} - 2\theta_i - \theta_j\right) + \frac{EA}{35}\left(\frac{9v_i^2}{l^2} - \frac{18v_iv_j}{l^2} + \frac{6v_i\theta_i}{l} + \frac{9v_j^2}{l^2}\right.$$
$$\left. - \frac{6v_j\theta_j}{l} + \frac{\theta_i^2}{4} + \frac{v_i\theta_j}{4} - \frac{\theta_j^2}{4}\right) \tag{20f}$$

$$a_7 = \frac{EB}{5l}\left(-2v_i + 2v_j + \frac{10\theta_i l}{3} - \frac{\theta_j l}{3}\right) + \frac{EA}{35}\left(\frac{3v_i^2}{l} - \frac{6v_iv_j}{l} - \frac{v_i\theta_i}{2} + \frac{v_i\theta_j}{2}\right.$$
$$\left. + \frac{3v_j^2}{l} + \frac{v_j\theta_i}{2} - \frac{v_j\theta_j}{2} + 2\theta_i^2 l - \frac{\theta_i\theta_j l}{2} + \frac{\theta_j^2 l}{6}\right) \tag{20g}$$

$$a_8 = \frac{EB}{5}\left(\frac{\theta_i}{6} - \frac{\theta_j}{6}\right) + \frac{EA}{35}\left(\frac{v_i\theta_i}{2} - \frac{v_j\theta_i}{2} + \frac{v_i\theta_j}{2} - \frac{v_j\theta_j}{2} - \frac{\theta_i^2 l}{4} + \frac{\theta_i\theta_j l}{3} - \frac{\theta_j^2 l}{4}\right) \tag{20h}$$

$$a_9 = \frac{EB}{5l}\left(2v_i - 2v_j - \frac{\theta_i l}{3} - \frac{10\theta_j l}{3}\right) + \frac{EA}{35}\left(\frac{3v_i^2}{l} - \frac{6v_iv_j}{l} + \frac{v_i\theta_i}{2} - \frac{v_i\theta_j}{2}\right.$$
$$\left. + \frac{3v_j^2}{l} - \frac{v_j\theta_i}{2} + \frac{v_j\theta_j}{2} + 2\theta_j^2 l - \frac{\theta_i\theta_j l}{2} + \frac{\theta_i^2 l}{6}\right) \tag{20i}$$

4. Solution procedure

The structure equilibrium equations are assembled in the global coordinate system, which is fixed in space, from contributions of all the beam elements. A load control or displacement control incremental method, combined with the Newton-Raphson iterative algorithm, can be applied to solve the nonlinear equilibrium equations. To facilitate the analysis of possible softening behaviour of a beam, an incremental arc-length method with the following arc-length constraint

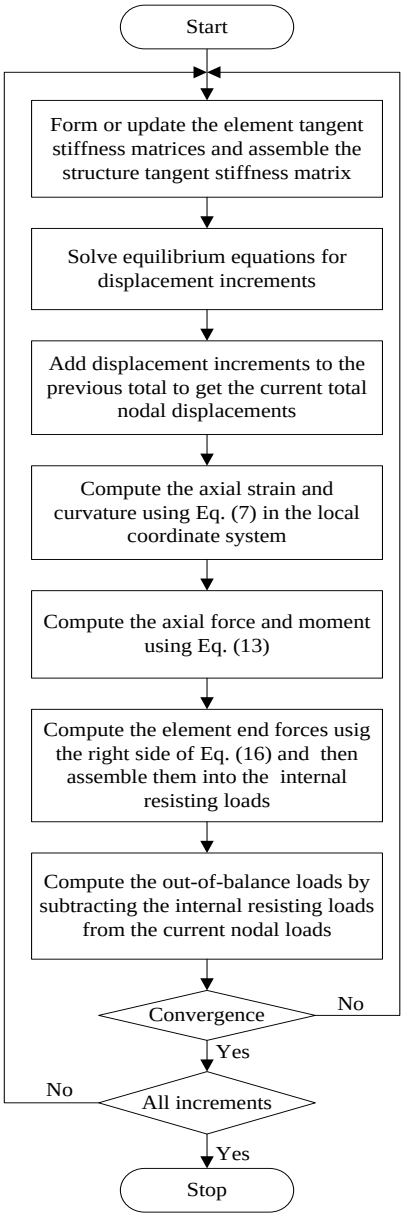

Fig. 3 Flow chart of solution procedure

equation (Lam and Morley 1992) is incorporated into the computer model.

$$\Delta \boldsymbol{u}_1^T \delta \boldsymbol{u}_i + \Delta\lambda_1 \delta\lambda_i \boldsymbol{P}^T \boldsymbol{P} = 0 \tag{21}$$

where $\boldsymbol{P}$ is the specified nodal loads; $\delta \boldsymbol{u}_i = \Delta \boldsymbol{u}_{i+1} - \Delta \boldsymbol{u}_i$; $\delta\lambda_i = \Delta\lambda_{i+1} - \Delta\lambda_i$; $\Delta \boldsymbol{u}_i$ is the nodal displacement increments after the *i*th iteration; and $\Delta\lambda_i$ is the incremental load factor after the *i*th iteration.

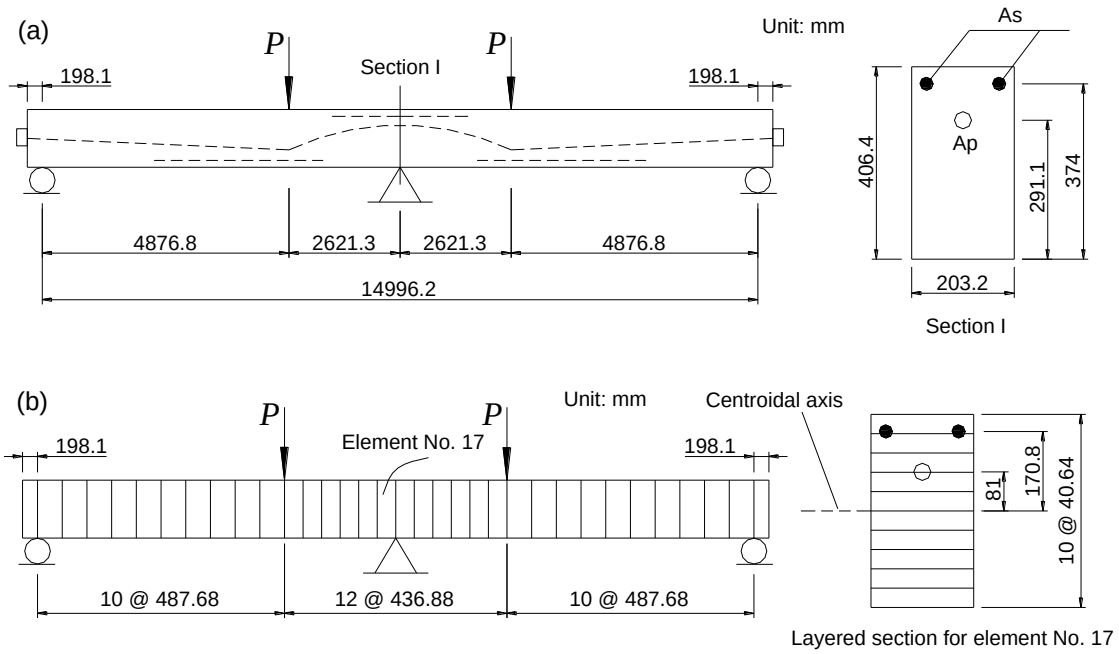

Fig. 4 Experimental beams by Lin (1955) and their finite element model. (a) details of the experimental beams; (b) finite element model

The iterative procedure for each increment involves four basic steps: (1) form the current tangent stiffness matrix; (2) solve the equilibrium equations; (3) determine the current state for each element; and (4) check convergence. During the solution process, when any of the constituent materials (concrete, nonprestressed steel and prestressing steel) reaches its ultimate strain, the failure of the beam is assumed to take place and the analysis is therefore terminated. A summary of the solution procedure involved in the nonlinear computer analysis is given in the flow chart of Fig. 3.

A computer programme which implements the above described numerical procedure is developed. The numerical procedure takes into account both the geometric and material nonlinearities, and is capable of predicting the comprehensive aspects of nonlinear behaviour of continuous bonded prestressed concrete beams throughout all stages of loading up to failure. To illustrate the reliability and applicability of the proposed method of analysis, some numerical examples are presented in the following section.

5. Numerical applications

5.1 Analysis of Lin beams

In an experimental programme performed by Lin (1955), four bonded prestressed concrete continuous beams were tested under static or repeated loads up to failure. These experimental beams were fabricated in large sizes, and the tests were well executed. Two of the beams,

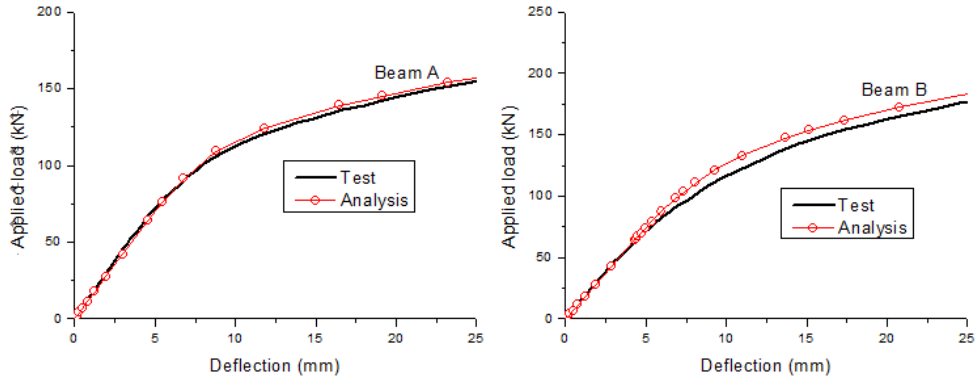

Fig. 5 Comparison between numerical and experimental results regarding the load-deflection response for Beams A and B

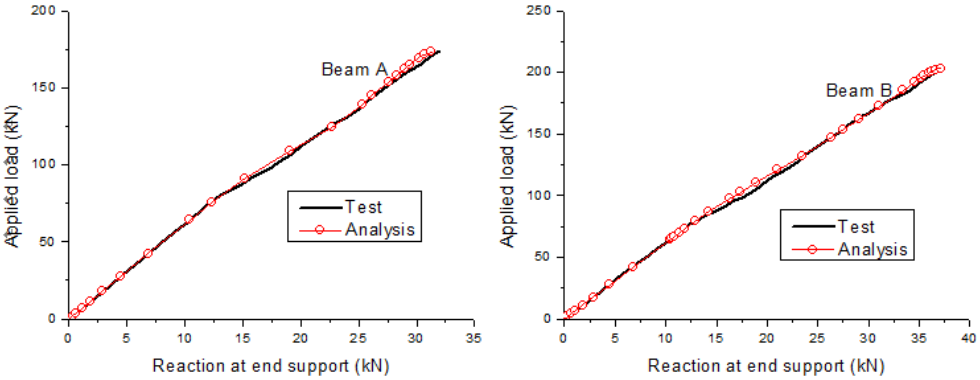

Fig. 6 Comparison between numerical and experimental results regarding the load-reaction response for Beams A and B

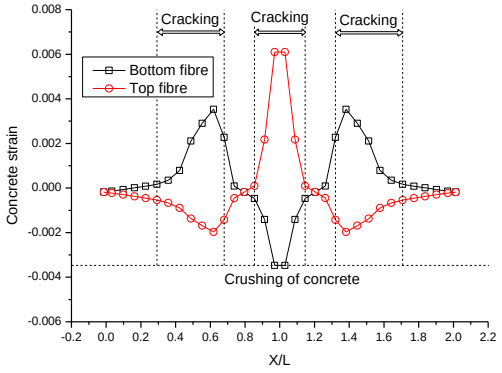

(a)

Fig. 7 Concrete strain distribution along the beam length. (a) Beam A; (b) Beam B

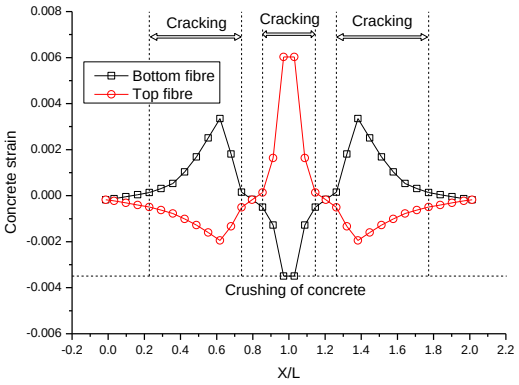

(b)

Fig. 7 Continued

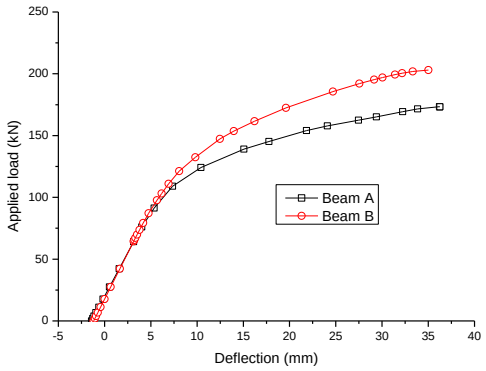

(a)

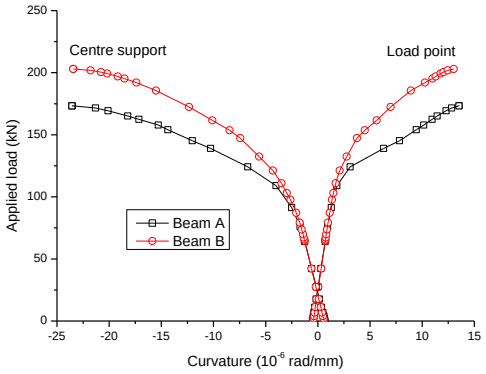

(b)

Fig. 8 Loa-deformation characteristics for Beams A and B. (a) load-deflection response; (b) load-curvature response

designated as Beams A and B and tested under static loads, are analyzed in this study. These two beams were identical except the content of nonprestressed steel: Beam B contained two 14 mm mild steel bars over the critical positive and negative regions while Beam A did not. The dimensions and steel layouts are shown in Fig. 4(a). The beams were of a rectangular cross section, 203.2 mm wide and 406.4 deep, and were continuous over two equal spans of 7498.1 mm each. Two concentrated loads were symmetrically applied at points at a distance of 4876.8 mm from end supports. The tendon profile for each span consisted of a straight part and a curve part, and the tendon line was designed to be concordant.

The prestressing steel, consisted of 32 parallel wires of 5 mm diameter, had an ultimate strength of 1765 MPa, a yield stress of 1572 MPa and an elastic modulus of 200 GPa. The nonprestressed steel had a yield stress of 314 MPa and an elastic modulus of 196 GPa. The concrete cylinder compressive strengths for Beams A and B were 36.2 and 41.3 MPa, respectively. At time of loading, the effective prestress after all prestress losses was 827.4 MPa.

The finite element model of the beams is shown in Fig. 4(b). The concrete beam is divided into 34 beam elements and the element is subdivided into 10 concrete layers, one tendon layer representing the prestressing steel and, if any, one nonrestressed steel layer representing the top or bottom steel bars. Figs. 5 and 6 show the comparisons between model predictions and experimental results in relation to the load-deflection response and load-reaction response, respectively. The deflections are plotted up to 25 mm (experimental data beyond this value were not reported). Because the experimental results were reported without the initial values, the predicted deflections and reactions are shifted to corresponding values in accordance with zero cambers and initial reactions. From Fig. 5, it is seen that the predicted load-deflection characteristics for Beam A are in excellent agreement with the experimental results; for Beam B, although the predicted values tend to be a little stiffer than the experimental ones in the post-elastic stage, favourable comparison can also be observed. From Fig. 6, it can be seen that the numerical analysis reproduces the load-reaction behaviour of the beams, from zero loads up to failure, with remarkable accuracy. The analysis shows that the beams have failed due to the crushing of concrete over the centre support. This failure mode is consistent with the experimental observation. The predicted ultimate loads for Beams A and B are respectively 173.3 and 203.0 kN, which are in very good agreement with the corresponding experimental values of 174.4 and 203.7 kN.

Fig. 7 illustrates the concrete strain distribution at extreme compression and tension fibres along the length of the beams, X/L (ratio of the distance from the end support to the span), at failure. It is seen that when the concrete at the centre support is crushed, the span critical section (load point) is still far away from its full rotation capacity. Both beams exhibits favourable crack pattern. Due to the presence of nonprestressed steel, Beam B displays larger cracking zone but a little smaller crack width than does Beam A.

Fig. 8(a) and (b) show load-deflection response and load-curvature response, respectively. Prior to cracking, the difference between deformations of the two beams is negligible, indicating that the effect of nonprestressed steel is insignificant in this elastic stage. After cracking, the effect of nonprestressed steel becomes increasingly important. As a consequence, Beam B is stiffer than Beam A. At the ultimate state, the deformations of Beam B are lower than those of Beam A. In addition, as indicated in the load versus curvature curves for the two critical sections (Fig. 8(b)), the centre support section attains its ultimate rotation capacity while the load point section reaches a level well below the ultimate capacity.

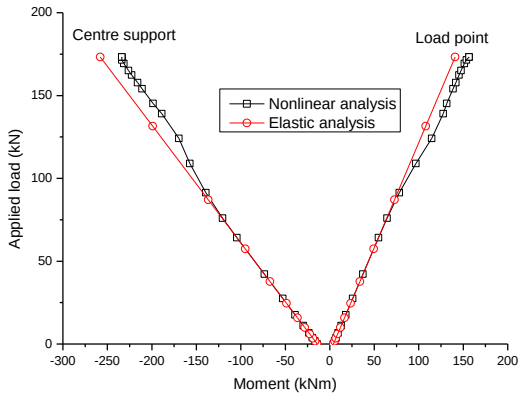

(a)

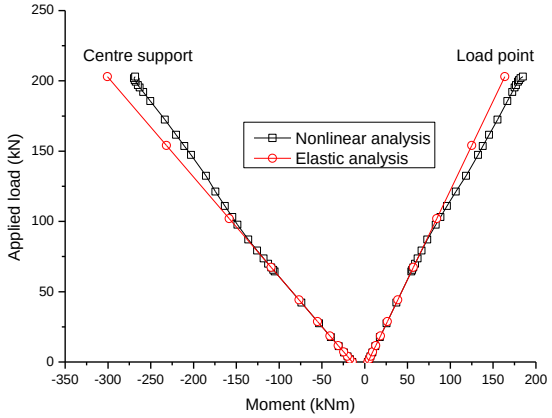

(b)

Fig. 9 Development of moments in specimens. (a) Beam A; (b) Beam B

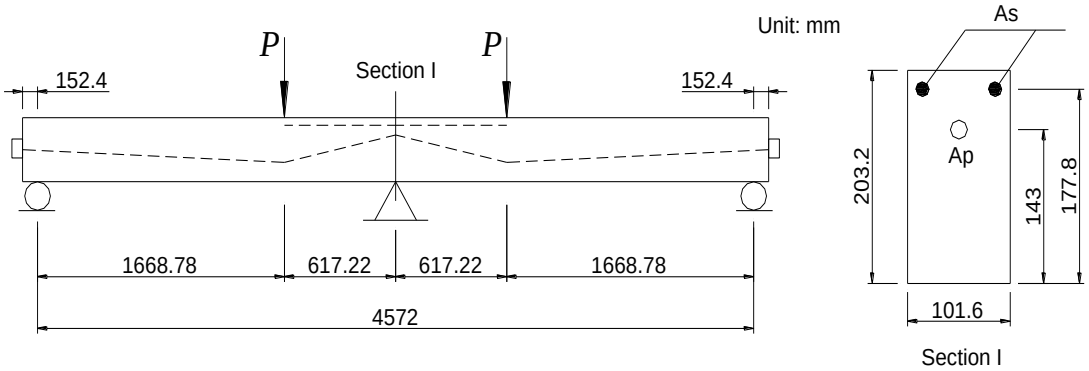

Fig. 10 Details of the experimental beam by Mallick (1962)

Table 1 Values of the actual moment, elastic moment and the degree of moment redistribution for Beams A and B

Beam	Actual moment M (kN·m)		Elastic moment M_e (kN·m)		Degree of redistribution (1-M/M_e) (%)	
	Centre support	Load point	Centre support	Load point	Centre support	Load point
A	-233.82	156.51	-257.98	140.80	9.36	-11.16
B	-268.26	184.74	-300.58	163.71	10.75	-12.84

Fig. 9(a) and (b) illustrate the development of moments for the two critical sections of Beams A and B, respectively. Both the actual values, obtained from the proposed nonlinear finite element analysis, and the elastic values, computed from an elastic analysis, are presented. At initial loading up to first cracking, the actual and elastic moment developments are identical and exhibit linear behaviour, indicating that the moment redistribution does not yet take place. After cracking, the actual moments deviate from the elastic values, attributed to the redistribution of moments. The actual moments, elastic moments and the degrees of moment redistribution for the two beams at failure are given in Table 1. It is seen that, despite the presence of nonprestressed steel, Beam B registers higher redistribution of moments compared to Beam A. This observation implies that the moment redistribution in a continuous beam depends not only on the ductility of one critical section but also on the structural characteristics of the whole member.

5.2 Analysis of Mallick beam

Mallick (1962) tested a number of two-span continuous bonded prestressed concrete beams to examine the moment redistribution in the beams. One of the beams, designated as Beam P4, is selected for the present analysis. The details of the beam are illustrated in Fig. 10. The main material parameters are as follows: f_{ck} = 34.2 MPa; A_p = 81.07 mm^2; f_{pu} = 1548 MPa; f_{py} = 1316 MPa; E_p = 202 GPa; A_s = 63.3 mm^2; f_y = 310.3 MPa; E_s = 207 GPa. The effective prestress f_{pe} = 876 MPa.

According to the model prediction, failure of the beam takes place when the concrete at the centre support is crushed. The experiment exhibited the same failure mode. The predicted failure load is 55.6 kN, which is slightly higher than the experimental value of 53.4 kN. The predicted ultimate moment at the load point section is 11.5 kN·m, which is a bit smaller than the corresponding experimental value of 12.0 kN·m, while the predicted ultimate moment at the centre support is 18.5 kN·m against the experimental value of 16.5 kN·m. This discrepancy between the predicted and experimental results can be attributed to that some of the material parameters used in the analysis are determined using the empirical equations and, therefore, may be different from the actual values for the test. For example, most of the material parameters related to the concrete, including the concrete modulus of elasticity, ultimate compressive stain and the concrete tensile strength, are calculated in terms of the concrete compressive strength using the empirical equations described in Section 2. Although there are some slight errors, the results obtained from the proposed analysis are in favourable agreement with the experimental data.

Fig. 11 shows the development of moments at the centre support and load point and the evolution of the moment ratio (ratio of the moment at the centre support to the moment at the load point) for the experimental beam. Prior to cracking, there is no redistribution of moments and,

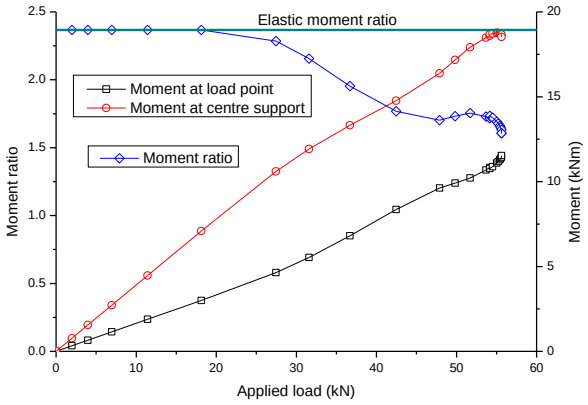

Fig. 11 Development of moments and moment ratio for the experimental beam

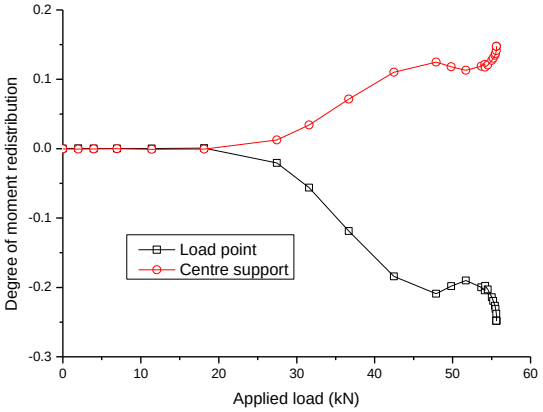

Fig. 12 Variation of the degree of moment redistribution with the applied load for the experimental beam

therefore, the moments develop linearly with the applied load and the moment ratio is equal to the elastic value of 2.37, as can be seen in Fig. 11. After cracking, the moment redistribution takes place. As a consequence, the load-moment relationship exhibits nonlinear behaviour and the moment ratio deviates from the elastic value. Because the first crack appears at the centre support, upon cracking the moment tends to be redistributed from the centre support section to the span critical section, leading to a diminution of the rate of increase in the moment for the centre support section and a consequent growth of the rate for the load point section. As a result, the moment ratio decreases. The evolution of the moment ratio reflects the progress of the moment redistribution in the beam.

Fig. 12 demonstrates the development of the degree of moment redistribution defined by $(1-M/M_e)$, where M is the actual moment and M_e is the elastic moment. It is seen that the degree of moment redistribution is equal to zero until the first cracking takes place. Beyond the

cracking load, there is positive redistribution of moments at the centre support but negative one at the load point. After cracking, the redistribution increases quickly until the nonprestressed steel over the centre section reaches its yield stress. This is followed by a slight decrease in the redistribution and soon after by a quick increase again in the redistribution up to failure of the beam.

6. Conclusions

A finite element model for the complete nonlinear analysis of bonded prestressed concrete continuous beams has been developed. The model is based on the Euler-Bernoulli beam theory and accounts for both geometric and material nonlinearities. The stiffness matrix, established according to the total Lagrangian description, consists of three submatrices, namely, the material stiffness matrix representing the material nonlinearity, the geometric stiffness matrix representing the geometric nonlinearity as a result of the axial force, and the large displacement stiffness matrix representing the large displacement effects. An incremental arc-length method, combined with the Newton-Raphson iterative algorithm, is used to trace the entire nonlinear equilibrium path of the structure. The proposed model is able to simulate the comprehensive behaviour of continuous bonded prestressed concrete beams over the complete loading stage up to the ultimate failure. The reliability and applicability of the model have been verified through the analysis of some experimental beams available in literature. The analysis reproduced the experimental results of the continuous beams with favourable agreement. In addition, some typical aspects of nonlinear behaviour of the beams were examined.

It is believed with confidence that the proposed model can be applied to an extensive numerical investigation of the inelastic behaviour of continuous beams which has not yet been fully understood, such as the redistribution of moments in normal and high-strength concrete beams prestressed with conventional and nonconventional tendons. Such an investigation is being performed to increase the depth of understanding of behaviour of these beams (Lou *et al*. 2015).

Acknowledgements

This research is sponsored by FEDER funds through the programme COMPETE (Programa Operacional Factores de Competitividade) and by national funds through FCT (Fundação para a Ciência e a Tecnologia) under the project PEst-C/EME/UI0285/2013. The work presented in this paper has also been supported by FCT under Grant No. SFRH/BPD/66453/2009.

References

Al-Sadder, S.Z., Othman, R.A. and Shatnawi, A.S. (2006), "A simple finite element formulation for large deflection analysis of nonprismatic slender beams", *Struct. Eng. Mech.*, **24**(6): 647-664.

Campbell, T.I. and Kodur, V.K.R. (1990), "Deformation controlled nonlinear analysis of prestressed concrete continuous beams", *PCI J.*, **35**(5): 42-55.

CEN (2004), "Eurocode 2 (EC2): Design of concrete structures – Part 1-1: General rules and rules for buildings", EN 1992-1-1, European Committee for Standardization, Brussels, Belgium.

Ho, J.C.M. and Zhou, K.J.H. (2011), "Minimum deformability design of high-strength concrete beams in

non-seismic regions", *Comput. Concr.*, **8**(4), 445-463.
Kodur, V.K.R. and Campbell, T.I. (1996). "Evaluation of moment redistribution in a two-span continuous prestressed concrete beam", *ACI Struct. J.*, **93**(6), 721-728.
Kodur, V.K.R. and Campbell, T.I. (1999), "Factors governing redistribution of moment in continuous prestressed concrete beams", *Struct. Eng. Mech.*, **8**(2): 119-136.
Kulprapha, N. and Warnitchai, P. (2012), "Structural health monitoring of continuous prestressed concrete bridges using ambient thermal responses", *Eng. Struct.*, **40**: 20-38.
Lam, W.F. and Morley, C.T. (1992), "Arc-length method for passing limit points in structural calculation", *ASCE J. Struct. Eng.*, **118**(1), 169-185.
Lee, H.W., Barnes, R.W. and Kim, K.Y. (2004), "A continuity method for bridges constructed with precast prestressed concrete girders", *Struct. Eng. Mech.*, **17**(6), 879-898.
Lin, T.Y. (1955), "Strength of continuous prestressed concrete beams under static and repeated loads", *ACI J.*, **26**(10): 1037-1059.
Lou, T., Lopes, S.M.R. and Lopes, A.V. (2013a), "Flexural response of continuous concrete beams prestressed with external tendons", *ASCE J. Bridge Eng.*, **18**(6): 525-537.
Lou, T., Lopes, S.M.R. and Lopes, A.V. (2013b), "Nonlinear and time-dependent analysis of continuous unbonded prestressed concrete beams", *Comput. Struct.*, **119**, 166-176.
Lou, T., Lopes, S.M.R. and Lopes, A.V. (2014a), "External CFRP tendon members: Secondary reactions and moment redistribution", *Compos. Part B: Eng.*, **57**, 250-261.
Lou, T., Lopes, S.M.R. and Lopes, A.V. (2014b), "Flexure of continuous HSC beams with external CFRP tendons: Effects of fibre elastic modulus and steel ratio", *Compos. Struct.*, **116**, 29-37.
Lou, T., Lopes, S.M.R. and Lopes, A.V. (2014c), "FE modeling of inelastic behavior of reinforced high-strength concrete continuous beams", *Struct. Eng.Mech.*, **49**(3), 373-393.
Lou, T., Lopes, S.M.R. and Lopes, A.V. (2015), "A comparative study of continuous beams prestressed with bonded FRP and steel tendons", *Compos. Struct.*, http://dx.doi.org/10.1016/j.compstruct.2015.01.009
Mallick, S.K. (1962), "Redistribution of moments in two-span prestressed concrete beams", *Mag. Concrete Res.*, **14**(42), 171-183.
Markovic, M., Krauberger, N., Saje, M., Planinc, I. and Bratina, S. (2013), "Non-linear analysis of pre-tensioned concrete planar beams", *Eng. Struct.*, **46**, 279-293.
Menegotto, M. and Pinto, P.E. (1973), "Method of analysis for cyclically loaded reinforced concrete plane frames. IABSE preliminary report for symposium on resistance and ultimate deformability of structures acted on well-defined repeated loads", Lisbon, Portugal, 15-22.
Naito, C., Sause, R. and Thompson, B. (2008), "Investigation of damaged 12-year old prestressed concrete box beams", *ASCE J. Bridge Eng.*, **13**(2), 139-148.
Rana, S., Islam, N., Ahsan, R. and Ghani, S.N. (2013), "Application of evolutionary operation to the minimum cost design of continuous prestressed concrete bridge structure", *Eng. Struct.*, **46**, 38-48.
Roth, M.J., Slawson, T.R. and Flores, O.G. (2010), "Flexural and tensile properties of a glass fiber-reinforced ultra-high-strength concrete: an experimental, micromechanical and numerical study", *Comput. Concr.*, **7**(2), 169-190.
Schmidt, J.W., Bennitz, A., Taljsten, B., Goltermann, P. and Pedersen, H. (2012), "Mechanical anchorage of FRP tendons – A literature review", *Constr. Build. Mater.*, **32**: 110-121.
Turmo, J., Ramos, G. and Aparicio, A.C. (2011), "Structural behaviour of segmental concrete continuous bridges with unbonded prestressing and dry joints", *Struct. Infrastr. Eng.*, **7**(11), 857-868.